J. Appl. Comput. Mech., xx(x) (2026) 1-19
DOI: 10.22055/jacm.2026.48790.5501

ISSN: 2383-4536
jacm.scu.ac.ir

Shahid Chamran University of Ahvaz

Journal of Applied and Computational Mechanics

Research Paper

Study on the Effect of Profile Shifts on the Meshing Stiffness of Helical Gears

Lei Bu[1], Jingang Liu[1], Daqing Zhang[2], Yumin He[3], Wei Zhang[1], Bohuan Tan[1]

[1] School of Mechanical Engineering, Xiangtan University, Xiangtan 411105, China
[2] Sunward Intelligent Equipment Co., Ltd, Changsha 410000, China
[3] Xiangtan Electric Manufacturing Co., Ltd, Xiangtan 411105, China

Received September 28 2025; Revised December 05 2025; Accepted for publication January 26 2026.
✉ Corresponding author: J. Liu (liujingang@xtu.edu.cn)

Abstract. Time-varying meshing stiffness (TVMS) is a primary excitation source of vibration and noise in helical gear systems. However, the effect of profile modification coefficients on TVMS remains insufficiently investigated. A novel analytical model for the TVMS of profile-shifted helical gears is proposed, which integrates the slice theory and tooth profile generation principles. This model incorporates both equidistant and non-equidistant profile shift design schemes and analyses the TVMS of helical gear pairs under positive, negative, and zero profile shifting conditions to reveal how modification coefficients affect the TVMS of helical gears. The results indicate that: Among multiple gear pairs with the same centre distance, those with a smaller modification coefficient on the pinion than on the gear exhibit higher TVMS; When the centre distance increases uniformly relative to the standard value, gear pairs where the pinion's modification coefficient remains constant while the gear's increases achieve higher TVMS. These findings provide valuable references for the structural design and optimisation of helical gears.

Keywords: Profile shift; Helical gear; TVMS; Modification coefficients; Centre distance.

1. Introduction

The profile modification coefficient can adjust the meshing centre distance of helical gear systems to meet various practical application requirements. Consequently, profile-shifted helical gears are widely employed in electric drive assemblies for new energy vehicles [1]. Unlike traditional engines, electric drives lack a masking effect; coupled with growing user demand for quietness, this has attracted increasing attention to the NVH (Noise, Vibration, and Harshness) performance of helical gear systems [2]. Vibration and noise in profile-shifted helical gears are significantly affected by time-varying meshing stiffness (TVMS), as both TVMS and transmission error are time-varying during gear rotation and meshing [3, 4]. For an ideal helical gear pair, TVMS should be as high as possible with minimal fluctuation to suppress system vibration. Therefore, developing a computational model for the TVMS of helical gears and analysing the influence of modification coefficients are fundamental to investigating their vibration response.

Three primary methods exist for analysing gear TVMS: experimental, finite element, and analytical approaches [5, 6]. Specifically, the experimental method uses high-precision equipment to measure stress and displacement during gear rotation, which are then integrated with theoretical models to determine meshing stiffness. While this method ensures reliable computational accuracy, it requires substantial financial investment and lengthy testing cycles [7]. The finite element method discretises the gear into finite elements and computes TVMS by analysing deformation and profile shift under load; however, this method is computationally expensive, especially for multiple modified gear sets that require repeated modelling, mesh optimisation, and boundary condition matching [8, 9].

To address these challenges, the analytical method has been developed to balance computational efficiency, testing cost, and simulation accuracy. For instance, the potential energy method (PEM) models the gear cross-section as a variable-section cantilever beam fixed at the base circle, calculating bending, shear, compressive, and contact stiffness to sum into the TVMS of the gear pair [10, 11]. Alternatively, the "slice method" divides the gear along the tooth width, computes the meshing stiffness of each slice via PEM, and sums these individual stiffness values to obtain the overall TVMS [12].

When analysing the TVMS of helical gears using analytical methods, the helical gear is often modelled as multiple straight gears arranged axially. This approach requires careful consideration of varying numbers of meshing teeth and meshing lines. Particular attention must be paid to how modification coefficients influence the length of each meshing line [13]. Wan et al. [14] developed an engagement line identification model to calculate TVMS in standard helical gears. They analysed how the normal module and

Published online: February 19 2026

tooth surface cracks affect meshing stiffness. Feng et al. [15] introduced a method for converting contact lines into a time-varying pressure angle. This was used to model TVMS and to study the impact of helix angle and gear width on meshing stiffness behaviour. Hongbo et al. [16] included the difference between base circle and root circle radii in a TVMS model. Their study evaluated how flank clearance and the number of slices influence meshing stiffness. Overall, analytical methods for calculating gear TVMS primarily emphasise gear body structure and manufacturing factors, including asymmetric tooth geometries, tooth root profile variations during machining, flank clearance, tooth tip radius modifications, gear module, tooth width, and deformation interactions such as tooth root-tooth body coupling [17-22].

The essence of a profile-shifted gear lies in the alteration of the tooth profile. It is feasible to compute the TVMS of profile-shifted helical gears using analytical methods. Ma and Wang [23, 24] developed a TVMS model for profile shifted spur gears, studying the influence of modulation coefficients under both positive and negative conditions, with emphasis on variable centre distances. Tan et al. [25] established a TVMS calculation method for planetary spur gears that includes profile shift, analysing how single-gear profile shift affects system TVMS under variable centre distances. Yu et al. [26] proposed a TVMS model for asymmetric spur gears incorporating profile shift, and examined the effect of modification coefficients on the range of TVMS variation. When designing profile shift helical gear systems, it is essential to consider both variable and constant centre distance strategies. The appropriate modification coefficient must be selected from multiple sets to achieve higher meshing stiffness with minimal fluctuation.

This study develops a TVMS model for profile-shifted helical gears using the potential energy method and a slice-based approach. The TVMS response of multiple gear systems under profile shift conditions is analysed, comparing both variable and constant centre distance design strategies. The influence of the modification coefficient on TVMS is investigated, providing a theoretical basis for evaluating NVH performance in helical gear transmissions.

The main contributions are:

1. A novel TVMS analysis model for profile-shifted helical gear pairs is developed. It includes an instantaneous judgment unit that captures the effect of modification coefficients on time-varying contact lines and meshing tooth pairs, enabling comprehensive meshing stiffness analysis.
2. This study examines the influence of the profile modification coefficients of large and small gears on the TVMS of helical gear pairs under various conditions. These conditions include variable centre distance and constant centre distance design strategies, as well as positive profile shifting, negative profile shifting, and zero profile shifting. This indirectly shortens the NVH performance evaluation cycle of the helical gear transmission system.

The remainder of this paper is structured as follows: Section 2 presents the TVMS analysis model for helical gears, considering profile shift. Section 3 provides a validation of the theoretical model. Section 4 investigates and discusses the variations in helical gear meshing stiffness under different profile shift configurations. Finally, Section 5 summarises the conclusions. The analysis flowchart of this study is illustrated in Fig. 1.

2. Calculation of TVMS for Profile Shifted Helical Gears

2.1. Tooth profile curve of shift gear

In this section, a variable meshing stiffness model is developed for profile shifted helical gears. Figure 2 illustrates the machining process of a modified helical gear, where the red line represents the cutting path of a standard gear. When the x_{mc} is positive, the tool moves away from the gear centre, resulting in a tooth root thickness of the machined gear that is larger than that of the standard gear (green line in Fig. 2). Conversely, when the x_{mc} is negative, the tool moves toward the gear centre, resulting in a tooth thickness smaller than that of the standard gear (blue line in Fig. 2). As shown in Fig. 3, the tooth profile can be divided into four segments: the tip curve AB, the involute curve BC, the transition curve CD, and the root curve DE.

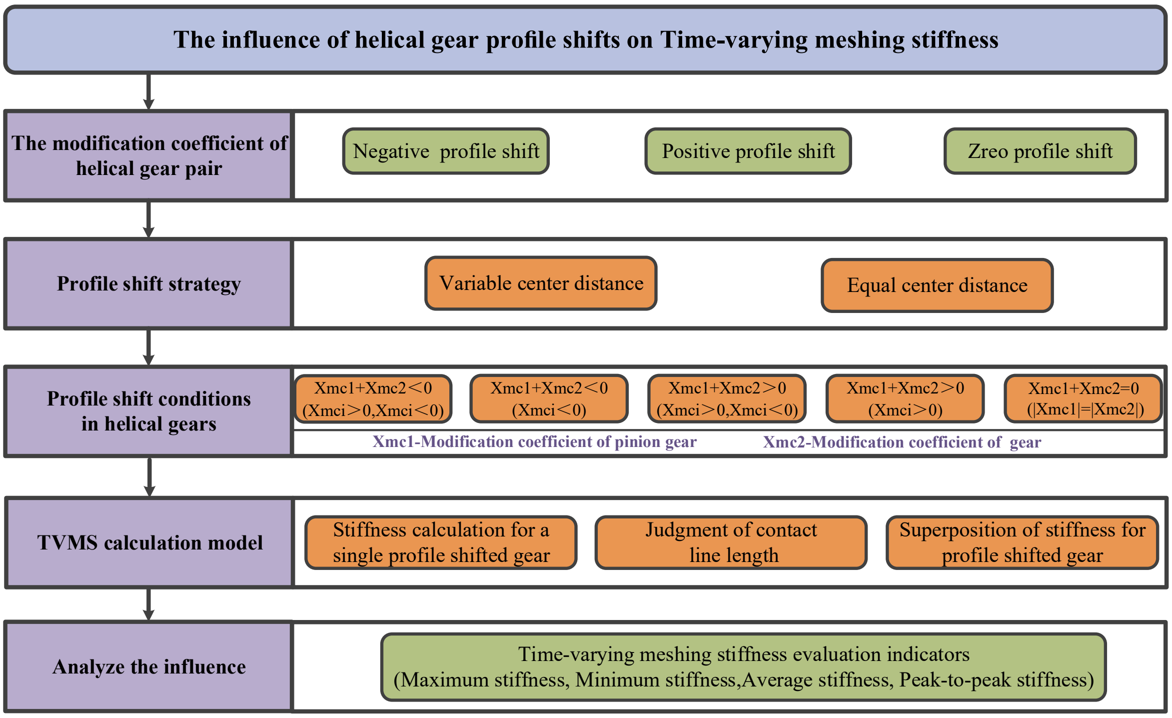

Fig. 1. Stiffness analysis considering profile shift.

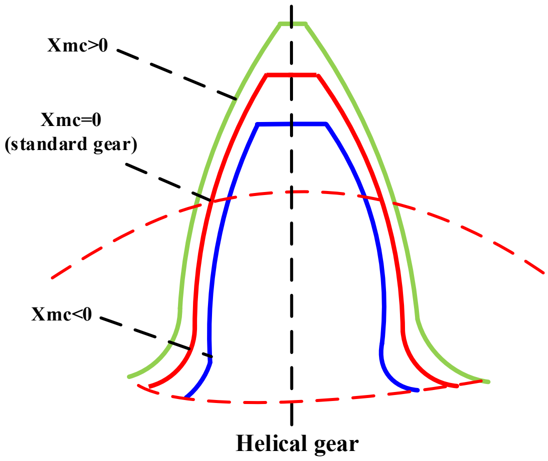

Fig. 2. Shift gear schematic diagram.

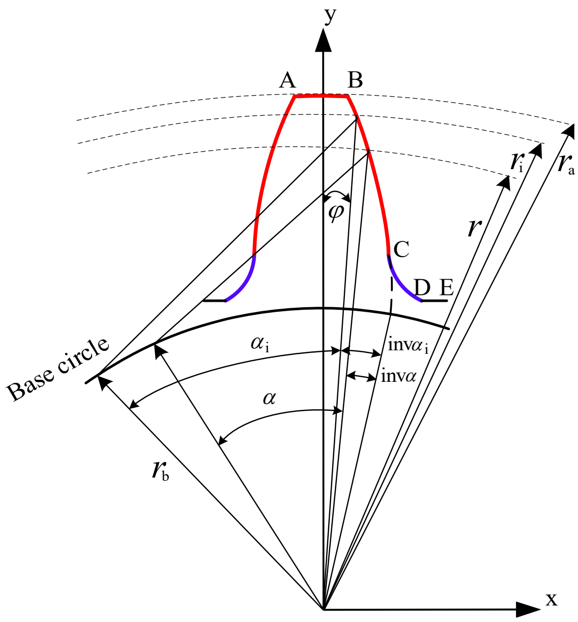

Fig. 3. Geometric model of gear profile.

The involute curve is described by the following equation [23]:

$$\begin{cases} x = r_i \sin\varphi \\ y = r_i \cos\varphi \end{cases} \tag{1}$$

$$\varphi = \left(2x_{mc}\tan\alpha + \frac{\pi}{2}\right)/Z - (\operatorname{inv}\alpha_i - \operatorname{inv}\alpha) \tag{2}$$

where $r_i = r_b / \cos\alpha_i$, $\alpha_i\,(\alpha_c \le \alpha_i \le \alpha_a)$ is the pressure angle at any point on the involute curve, $\alpha_c = \arccos(r_b / r_c)$, $\alpha_a = \arccos(r_b / r_a)$ are the pressure angles at the involute's initial point and the tip circle, respectively; $r_c = \sqrt{(r_b \tan\alpha - (h_a^* - x_{mc})m_n / \sin\alpha)^2 + r_b^2}$ is radius of the initial circle of the involute.

During the gear machining process, the cutting tool's motion trajectory generates both an involute curve (BC, shown in red in Fig. 3) and a transition curve (CD, shown in blue in Fig. 3). Although the transition curve CD does not directly contribute to the gear meshing process, its geometric properties play a crucial role in the accurate calculation of TVMS. The equation for this curve is given as [23]:

$$\begin{cases} x = r \times \sin(\Phi) - \left(a_1 / \sin\gamma + r_\rho\right) \times \cos(\gamma - \Phi) \\ y = r \times \cos(\Phi) - \left(a_1 / \sin\gamma + r_\rho\right) \times \sin(\gamma - \Phi) \end{cases} \quad (\alpha \le \gamma \le \pi / 2) \tag{3}$$

where $r_\rho = c^* m / (1 - \sin\alpha)$, $\Phi = (a_1 / \tan\gamma + b_1) / r$, $a_1 = \left(h_a^* + c^*\right)m - r_\rho - x_{mc}m$, $b_1 = \pi m / 4 + h_a^* m \tan\alpha + r_\rho \cos\alpha$.

2.2. Helical gear meshing stiffness model

As illustrated in Fig. 4, the helical gear is modeled as a straight-toothed gear along the tooth width direction, divided into multiple straight-toothed segments. The meshing stiffness of each segment is determined using the potential energy method.

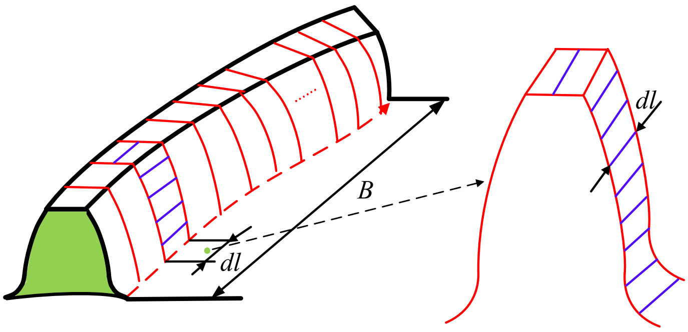

Fig. 4. Helical gear slicing diagram.

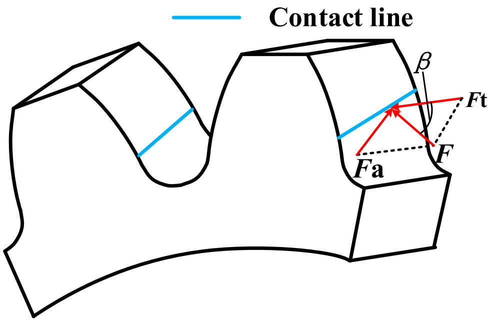

Fig. 5. Schematic diagram of the meshing forces in helical gears.

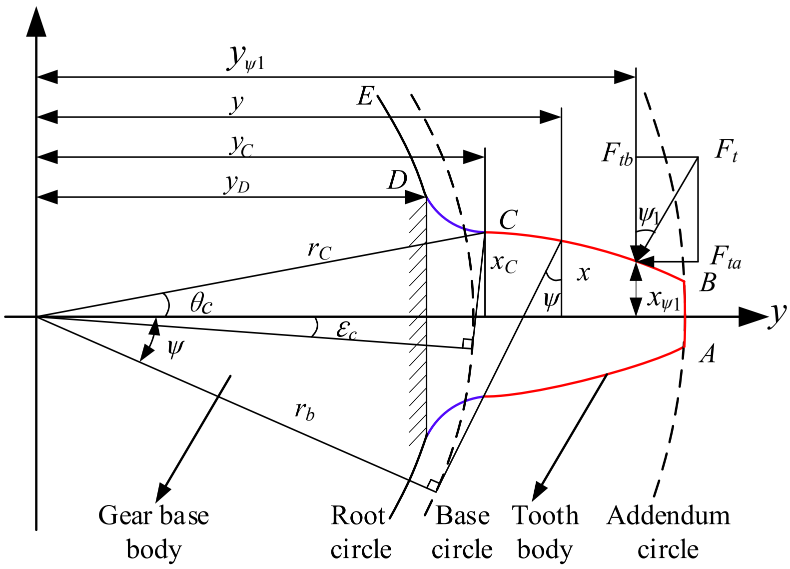

Fig. 6. Single-tooth profile geometric model.

The total TVMS of the helical gear pair is obtained by summing the stiffness values of all individual segments. The following assumptions are made in this paper: (1) The material is assumed to be homogeneous; (2) Friction, plastic deformation, and nonlinear effects are neglected; (3) The helical gear can be divided into N independent slices along the tooth width direction, where the coupling effects between adjacent slices are ignored, and the tooth stiffness of each slice can be calculated independently [11, 12].

2.2.1. *Gear tooth body stiffness*

During the meshing process of helical gear pairs, the contact line forms a certain spatial angle with the axis direction, known as the helix angle β. As shown in Fig. 5, the meshing force F can be orthogonally decomposed into: the tangential force F_t and the axial force F_a:

$$\begin{cases} F_t = F\cos\beta \\ F_a = F\sin\beta \end{cases} \tag{4}$$

M_{t1} and M_{t2} represent the torques on the transition curve CD and the involute curve BC, respectively, with the formulas as follows:

$$\begin{cases} F_{ta} = F_t\sin\psi_1 = F\cos\beta\sin\psi_1 \\ F_{tb} = F_t\cos\psi_1 = F\cos\beta\cos\psi_1 \end{cases} \tag{5}$$

$$\begin{cases} M_{t1} = F_{tb}(y_{\psi_1} - y_1) - F_{ta}x_{\psi_1} \\ M_{t2} = F_{tb}(y_{\psi_1} - y_2) - F_{ta}x_{\psi_1} \end{cases} \tag{6}$$

As shown in Fig. 6, the meshing stiffness of the tooth body includes the bending stiffness, shear stiffness, compressive stiffness, and Hertzian contact stiffness. The bending potential energy, shear potential energy, and compressive potential energy of the transition curve CD and the involute curve BC for a single tooth body are expressed as follows:

$$dU_b = \frac{F^2}{2dk_b} = \int_{y_D}^{y_C} \frac{M_{t1}^2}{2EI_{y1}} dy_1 + \int_{y_C}^{y_{\psi_1}} \frac{M_{t2}^2}{2EI_{y2}} dy_2 \tag{7}$$

$$dU_s = \frac{F^2}{2dk_s} = \int_{y_D}^{y_C} \frac{1.2F_{tb}^2}{2GA_{y1}} dy_1 + \int_{y_C}^{y_{\psi_1}} \frac{1.2F_{tb}^2}{2GA_{y2}} dy_2 \tag{8}$$

$$dU_a = \frac{F^2}{2dk_a} = \int_{y_D}^{y_C} \frac{F_{ta}^2}{2EA_{y1}} dy_1 + \int_{y_C}^{y_{\psi_1}} \frac{F_{ta}^2}{2EA_{y2}} dy_2 \tag{9}$$

where E, G, and υ represent Young's modulus, shear modulus, and Poisson's ratio, respectively. Specific values are shown in Table 2. The gear stiffness calculation considering profile shift employs the angular displacement method. The formulas for tooth body bending stiffness, tooth body shear stiffness, and tooth body compressive stiffness are as follows:

$$\frac{1}{dk_b} = \int_{\frac{\pi}{2}}^{\psi_t} \frac{\left[\cos\psi_1\left(y_{\psi_1} - y_1\right) - x_{\psi_1}\sin\psi_1\right]^2 \cos^2\beta}{EI_{y1}} \frac{dy_1}{d\gamma} d\gamma + \int_{\varepsilon_c}^{\psi_1} \frac{\left(\cos\psi_1\left(y_{\psi_1} - y_2\right) - x_{\psi_1}\sin\psi_1\right)^2 \cos^2\beta}{EI_{y2}} \frac{dy_2}{d\varepsilon} d\varepsilon \tag{10}$$

$$\frac{1}{dk_s} = \int_{\frac{\pi}{2}}^{\psi_t} \frac{1.2\cos^2\psi_1\cos^2\beta}{GA_{y1}} \frac{dy_1}{d\gamma} d\gamma + \int_{\varepsilon_c}^{\psi_1} \frac{1.2\cos^2\psi_1\cos^2\beta}{GA_{y2}} \frac{dy_2}{d\varepsilon} d\varepsilon \tag{11}$$

$$\frac{1}{dk_a} = \int_{\frac{\pi}{2}}^{\psi_t} \frac{\sin^2\psi_1\cos^2\beta}{EA_{y1}} \frac{dy_1}{d\gamma} d\gamma + \int_{\varepsilon_c}^{\psi_1} \frac{\sin^2\psi_1\cos^2\beta}{EA_{y2}} \frac{dy_2}{d\varepsilon} d\varepsilon \tag{12}$$

where ψ_t denotes the tangential working pressure angle, ψ_1 is the pressure angle at the contact point. The derivations of $x_1, x_2, y_1, y_2, \varepsilon_c, y_{\psi_1}, x_{\psi_1}$, $dy_1/d\gamma$, $dy_2/d\varepsilon$, $I_{y1}, I_{y2}, A_{y1}, A_{y2}$ are provided in Appendix A, while the definitions of all parameters are listed in Appendix B.

The contact stiffness of a single helical gear pair k_h is:

$$dk_h = \frac{\pi E dl}{4\left(1 - \nu^2\right)} \tag{13}$$

2.2.2. Gear base body stiffness

As shown in Figure 6, when gears are subjected to meshing forces, torsional deformation occurs in the gear base. The stiffness of the gear base is [27]:

$$\frac{1}{dk_f} = \frac{\cos^2\beta\cos^2\psi_1}{Edl}\left\{L^*\left(\frac{u_f}{S_f}\right)^2 + M^*\left(\frac{u_f}{S_f}\right) + P^*\left(1 + Q^*\tan^2\psi_1\right)\right\} \tag{14}$$

where $L^*, M^*, P^*, Q^*, u_f, S_f$ can be found in reference [27].

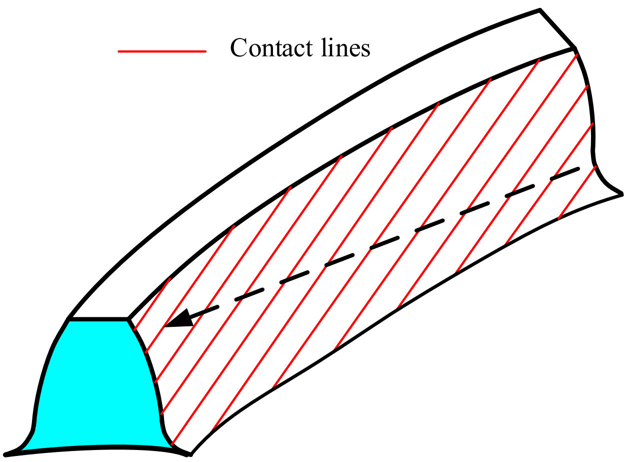

Fig. 7. The meshing characteristics of helical gears.

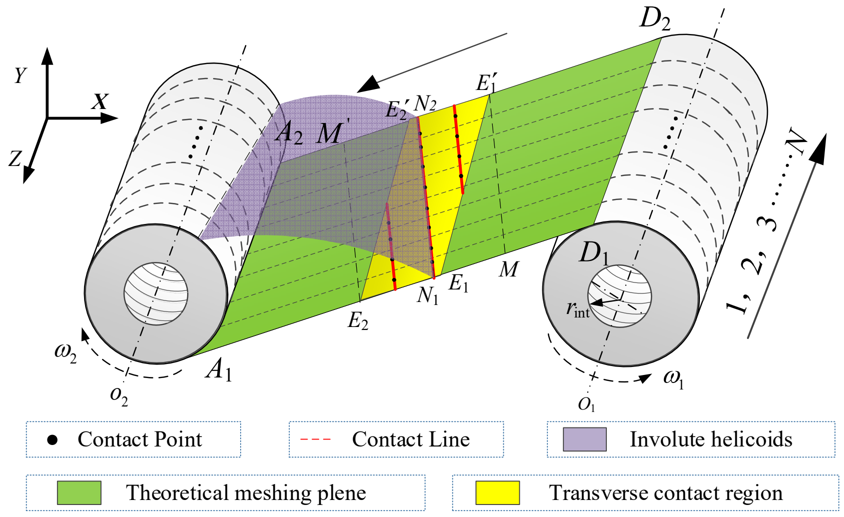

Fig. 8. Tooth-tooth engagement model.

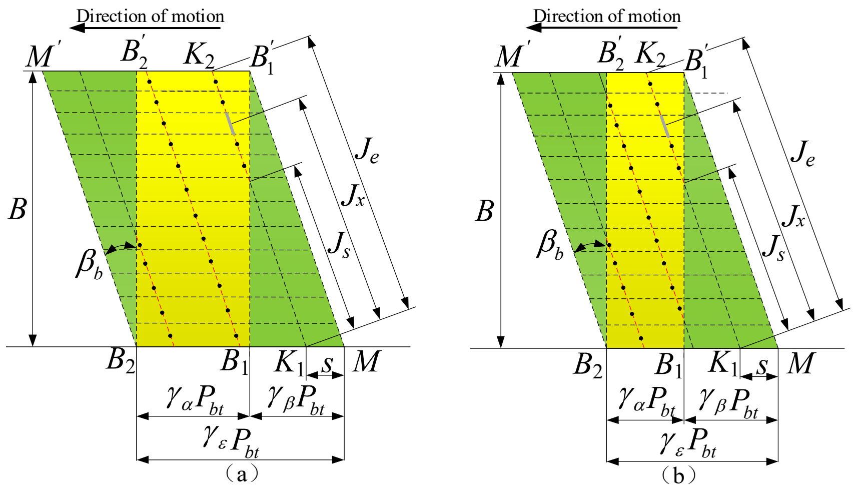

Fig. 9. Schematic diagram of contact wire movement: (a) $\gamma_\alpha \geq \gamma_\beta$, (b) $\gamma_\alpha < \gamma_\beta$.

2.3. Time-varying meshing stiffness considering profile shift

As shown in Fig. 7, the length of the contact line in a helical gear pair continuously changes during meshing. Therefore, when calculating the TVMS of a helical gear pair, it is essential to consider both the number of meshing gear pairs and the length of each contact line.

The helical gear is divided into multiple spur gears, and its meshing can be approximated by the meshing of these individual spur gears. The key challenge is to equivalently convert the instantaneous, gradually changing meshing line of the helical gear into the meshing line of spur gears. As shown in Fig. 8, a sliced helical gear meshing model is developed. The plane $D_1 D_2 A_2 A_1$ represents the theoretical meshing surface tangent to the base circles of the helical gear pair. The lateral contact zone is denoted by $E_1 E_1' E_2 E_2'$, while the line $N_1 N_2$ indicates the instantaneous contact line of the helical gear at a given moment during meshing.

As shown in Fig. 9, the overall contact ratio γ of helical gears is divided into the tangential overlap ratio γ_α and the axial overlap ratio γ_β. To calculate the instantaneous contact line length and the number of teeth in mesh for the gear pair, a model for determining the overlap ratio and contact line is introduced. The motion trajectory of the contact line is represented by the motion factor z, which indicates the distance the contact line travels on the theoretical meshing plane $E_1E_1' E_2 E_2'$ [28]. The motion factor z is defined as:

$$z = r_{b1} \operatorname{mod}\left(\theta_Z + (\mathrm{i}-1)2\pi / \mathrm{z}_{n1}, \operatorname{ceil}(\gamma_\varepsilon)\frac{2\pi}{\mathrm{z}_{n1}}\right) \tag{15}$$

where θ_Z, r_{b1}, z_{n1} represent the angular displacement, base circle radius, and number of teeth of Gear 1, respectively; i (i = 1,2, ..., $\operatorname{ceil}(\gamma_\varepsilon)$) denotes the i-th gear contact pair, corresponding to the i-th contact line.

The starting position (J_s) and ending position (J_e) of the contact line J for a helical gear pair are:

If $\gamma_\alpha \geq \gamma_\beta$:

$$\begin{cases} J_s = (\gamma_\beta p_b - z)/\sin\beta_b; J_e = b/\cos\beta_b, & 0 \leq z < \gamma_\beta p_b \\ J_s = 0; J_e = b/\cos\beta_b, & \gamma_\beta p_b \leq z < \gamma_\alpha p_b \\ J_s = 0; J_e = (\gamma_\varepsilon P_b - z)/\sin\beta_b, & \gamma_\alpha p_b \leq z < \gamma_\varepsilon p_b \\ J_s = 0; J_e = 0, & \gamma_\varepsilon p_b \leq s \leq ceil(\gamma_\varepsilon) p_b \end{cases} \tag{16}$$

If $\gamma_\alpha < \gamma_\beta$:

$$\begin{cases} J_s = (\gamma_\beta p_b - z)/\sin\beta_b; J_e = b/\cos\beta_b, & 0 \le z < \gamma_\alpha p_b \\ J_s = (\gamma_\beta p_b - z)/\sin\beta_b; J_e = (\gamma_\varepsilon P_b - z)/\sin\beta_b, & \gamma_\alpha p_b \le z < \gamma_\beta p_b \\ J_s = 0; J_e = (\gamma_\varepsilon P_b - z)/\sin\beta_b, & \gamma_\beta p_b \le z < \gamma_\varepsilon p_b \\ J_s = 0; J_e = 0, & \gamma_\varepsilon \le ceil(\gamma_\varepsilon) p_b \end{cases} \tag{17}$$

where: γ_ε, γ_α, γ_β represent the total contact ratio, tangential contact ratio, and axial contact ratio, respectively, where, $\gamma_\varepsilon = \gamma_\alpha + \gamma_\beta$; P_b, b and β_b denote the base circle pitch, tooth face width, and base circle helix angle, respectively. The length of the contact line J is: $J = J_e - J_s$.

The contact line J is divided into several contact line units by the slicing method. Setting the unit length of the contact line as Δj, the total number of units N is:

$$N = \text{ceil}\left(\frac{J_e - J_s}{\Delta j}\right) \tag{18}$$

The length of the nth contact line Δj_N element is:

$$\Delta j_N = (J_e - J_s) - (N-1)\Delta j \tag{19}$$

The position of point x in the contact wire unit on contact wire J_x is:

$$J_{xc} = \begin{cases} J_s + 0.5\Delta j + (c-1)\Delta j, & c = 1,2\ldots N-1 \\ J_s + (N-1)\Delta j + 0.5\Delta j_N, & c = N \end{cases} \tag{20}$$

As shown in Fig. 10, the instantaneous contact of helical gears can be modeled as two truncated cones oriented in opposite directions. The points on the contact line between Gear 1 and Gear 2 along the line J_{xi} can be represented by the curvature radius R_t:

$$\begin{aligned} R_{t1} &= r_{b1}\tan\alpha_i - r_{b2}(\tan\alpha_{a2} - \tan\alpha_i) - B\tan\beta_b + z \\ R_{t2} &= r_{b2}\tan\alpha_i + r_{b2}(\tan\alpha_{a2} - \tan\alpha_i) + B\tan\beta_b - z \end{aligned} \tag{21}$$

In the formula: r_{b2}, α_i, and α_{a2} represent the base circle radius, working pressure angle, and addendum transverse pressure of the gear 2, respectively. The radius of curvature at point X on the contact line can be derived as:

$$R_{txi} = R_{ti} + J_x \sin\beta_b, i = 1,2 \tag{22}$$

The tangential pressure angle at contact point X is:

$$\psi = \arctan\left(\frac{R_{txi}}{r_{bi}}\right), i = 1,2 \tag{23}$$

As shown in Fig. 11, the TVMS of a helical gear pair is the integral of the meshing stiffness along the contact line J of the sliced gear pair. Its calculation formula is:

$$k = \int_J \frac{1}{\frac{1}{k_{b1}} + \frac{1}{k_{s1}} + \frac{1}{k_{a1}} + \frac{1}{k_{b2}} + \frac{1}{k_{s2}} + \frac{1}{k_{a2}} + \frac{1}{k_h}} \tag{24}$$

where 1 denotes the pinion gear, and 2 denotes the gear.

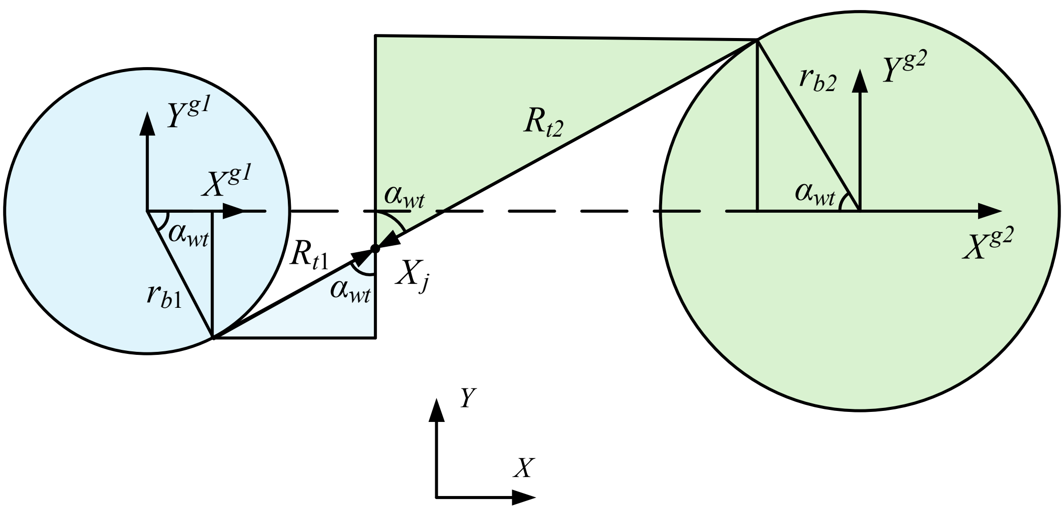

Fig. 10. Equivalent contact mechanics model.

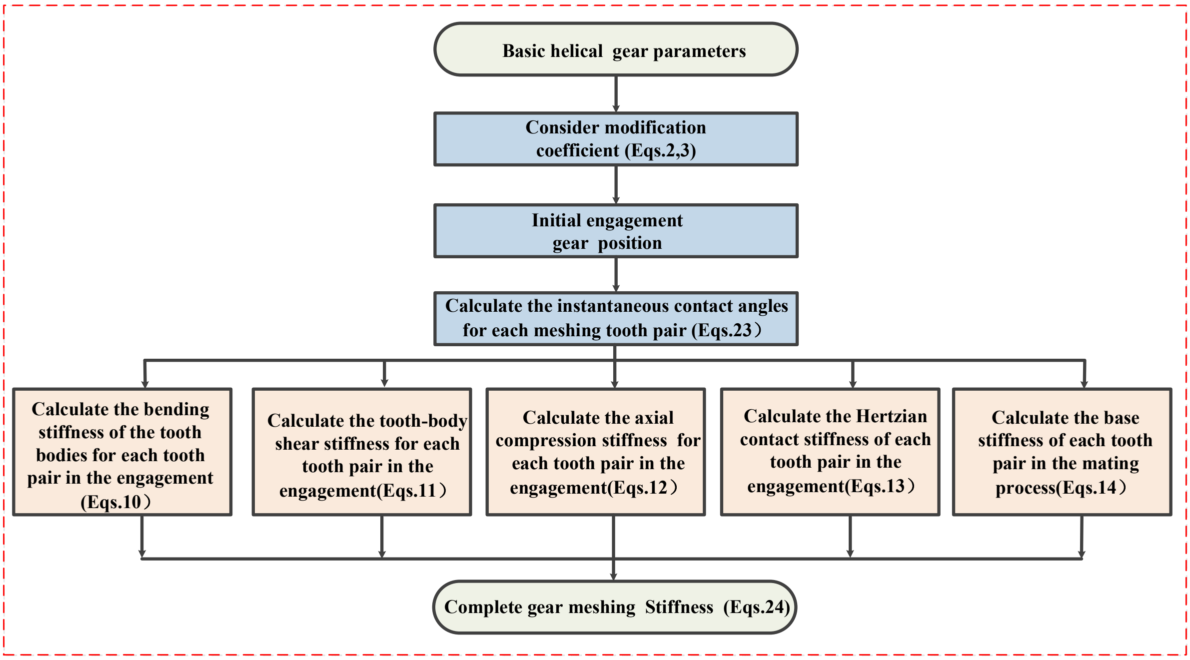

Fig. 11. Flowchart for calculating the TVMS of profile shifted helical gears.

3. TVMS Model Validation

In this section, a helical gear pair with a transmission ratio of i = 1.385 is used as an example. The TVMS data calculated in this study is compared with the data from Ma [13] to validate the proposed TVMS calculation model. The common parameters of the helical gear pair are listed in Table 1.

Table 2 presents the calculated results for maximum stiffness K_a and minimum stiffness K_b using both the proposed method and Ma's approach. As shown in Fig. 12 and Table 2, the relative error for K_a is 4%, while the relative error for K_b is 3%. The TVMS results for the helical gear obtained by this method closely match those calculated using Ma's TVMS method.

The comparison results between the proposed method, the finite element method (FEM), and experimental methods are shown in Table 3.

4. Analysis of Profile shift Coefficient Response to TVMS

Table 4 presents the variation patterns of TVMS for helical gear pairs with different profile shift coefficients, while keeping all other gear pair parameters constant, as specified in Table 1. As shown in Table 4, X_{mc1} refers to the modification coefficient of the pinion, and X_{mc2} refers to the modification coefficient of the gear.

Table 1. Basic Parameters of Helical Gear Pairs.

Gear parameter	Gear pair	
	Pinion	Gear
Number of Teeth	52	72
Module (mm)	1.75	1.75
Tooth Width (mm)	20	20
Pressure Angle (°)	20	20
Helix Angle (°)	20	20
Tooth Height Coefficient	1	1
Back Clearance Coefficient	0.25	0.25
Young's Modulus (Pa)	2.1×10^{11}	2.1×10^{11}
Poisson's Ratio	0.3	0.3
Center Radius (mm)	10	10

Table 2. Stiffness data comparison Table.

/	Stiffness Index	Propose method	Ma	Relative error
Gear pair	Minimum stiffness ($\times10^8$ N/m)	1.62	1.67	3%
	Maximum stiffness ($\times10^8$ N/m)	1.67	1.74	4%

Table 3. Comparison Table for stiffness calculation.

Method	Calculation Time	Hardware Cost
Proposed Method	No more than 10 seconds	Memory: 32 GB; Processor: Intel(R) Core(TM) i7-12700F @ 2.10 GHz; Operating System: Windows 10
Finite Element Method [11]	9.08 hours	Memory: 192 GB; Processor: Intel Xeon Gold 6258R CPU @ 2.70 GHz; Operating System: Windows 10
Experimental Method [7]	More than 2 minutes (Excluding experimental preparation time)	Complete measurement equipment required: including sensors, control system, test bench, etc.

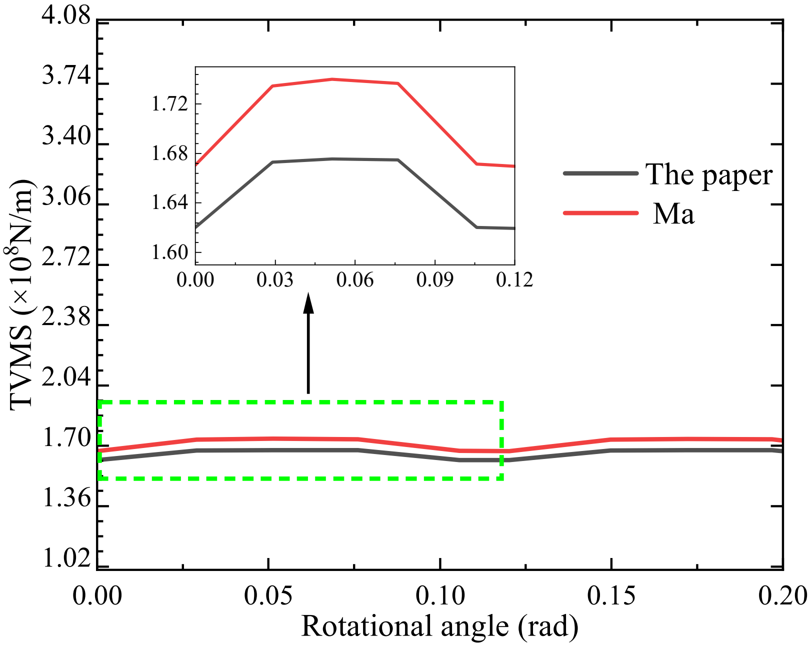

Fig. 12. Stiffness comparison chart.

This study focuses on three profile shift scenarios for helical gear pairs: positive profile shift (Tables 4-A.1 and A.2), negative profile shift (Tables 4-B.1 and B.2), and zero profile shift (Table 4-C). Within each scenario, two design strategies—variable centre distance and equal centre distance—are considered to examine how the profile shift coefficients of the large and small gears influence the TVMS of the gear pair. The specific effects of profile shift coefficients on TVMS are analyzed through metrics such as maximum stiffness (K_a), minimum stiffness (K_b), average stiffness (K_m), and peak-to-peak stiffness (K_{ppv}). This analysis provides a basis for quantitatively understanding the variation trends of TVMS in helical gear pairs.

The maximum stiffness K_a, minimum stiffness K_b, average stiffness K_m, and peak-to-peak stiffness K_{ppv} can be calculated using the following formula:

$$K_{\mathrm{m}} = \mathrm{mean}(K_{\mathrm{i}}) \tag{25}$$

$$K_{\mathrm{ppv}} = \max(K_{\mathrm{i}}) - \min(K_{\mathrm{i}}) \tag{26}$$

$$K_a = \max(K_{\mathrm{i}}) \tag{27}$$

$$K_{\mathrm{b}} = \min(K_{\mathrm{i}}) \tag{28}$$

4.1. Positive profile shift of helical gear

A.1. $X_{mci} > 0$ & $X_{mci} < 0$

As shown in Figs. 13(a), (c), (e), the first three combinations are as follows: X_{mc1} values of -0.1, -0.2, and -0.4, and corresponding X_{mc2} values of 0.2-0.5, 0.3-0.6, and 0.5-0.8, respectively. Figures 13(b), (d), and (f) display the last three combinations, which are the reverse of the previous ones.

Table 4. Gear shift parameter Table.

Gear Pair Sum of Profile shift Coefficients	Combination	Pinion gear (X_{mc1})	Large gear (X_{mc2})	Gear Pair Sum of Profile shift Coefficients	Combination	Pinion gear (X_{mc1})	Large gear (X_{mc2})
$X_{mc1} + X_{mc2} > 0$ ($X_{mci} > 0$, $X_{mci} < 0$)	A.1	-0.1	0.2~0.5	$X_{mc1} + X_{mc2} < 0$ ($X_{mci} > 0$, $X_{mci} < 0$)	B.1	0.1	-0.2~-0.5
		0.2~0.5	-0.1			-0.2~-0.5	0.1
		-0.2	0.3~0.6			0.2	-0.3~-0.6
		0.3~0.6	-0.2			-0.3~-0.6	0.2
		-0.4	0.5~0.8			0.4	-0.5~-0.8
		0.5~0.8	-0.4			-0.5~-0.8	0.4
$X_{mc1} + X_{mc2} > 0$ ($X_{mci} > 0$)	A.2	0.1	0.5~0.8	$X_{mc1} + X_{mc2} < 0$ ($X_{mci} < 0$)	B.2	-0.1	-0.3~-0.6
		0.5~0.8	0.1			-0.3~-0.6	-0.1
		0.2	0.4~0.7			-0.2	-0.2~-0.5
		0.4~0.7	0.2			-0.2~-0.5	-0.2
		0.3	0.3~0.6			-0.3	-0.1~-0.4
		0.3~0.6	0.3			-0.1~-0.4	-0.3
$X_{mc1} + X_{mc2} = 0$	C	0.1-0.4	-0.1~-0.4	/	/	/	/
		-0.1~-0.4	0.1-0.4	/	/	/	/

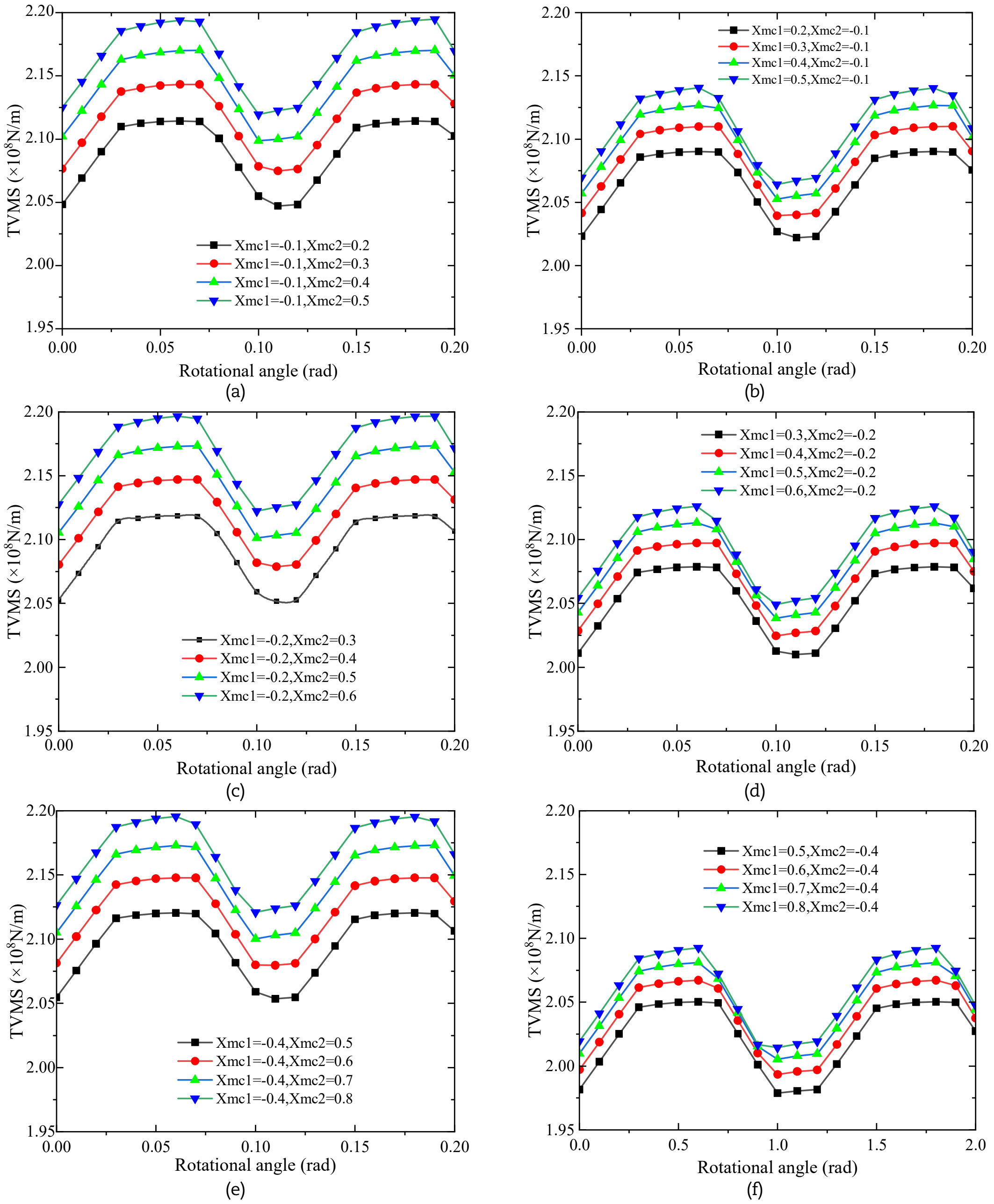

Fig. 13. TVMS with different modification coefficients.

As shown in Fig. 13, when the gear pair profile shift coefficients are identical (with consistent centre distances), the overall meshing stiffness is higher when $X_{mc1} < 0$ and $X_{mc2} > 0$ than when $X_{mc1} > 0$ and $X_{mc2} < 0$. For instance, the meshing stiffness of the combination $X_{mc1} = -0.4$, $X_{mc2} = 0.5$ (Fig. 13(e), black line) is higher than that of $X_{mc1} = 0.5$, $X_{mc2} = -0.4$ (Fig. 13(f), black line). As shown in Fig. 2, the gear tooth body cross-sectional area of the gear pair in the former combination is larger, thus the TVMS of the gear pair is greater.

When the increase amplitude of the profile modification coefficient of the helical gear pair (i.e., the increase amplitude of the centre distance) is consistent, the gear pair combination with $X_{mc1} < 0$ (constant) and $X_{mc2} > 0$ (gradually increasing) achieves a greater improvement in meshing stiffness than the opposite combination with $X_{mc2} < 0$ (constant) and $X_{mc1} > 0$ (gradually increasing). For example, a comparison between the combination of $X_{mc1} = -0.4$, $X_{mc2} = 0.5/0.6$ (Fig. 13(e), black and red lines) and the combination of $X_{mc2} = -0.4$, $X_{mc1} = 0.5/0.6$ (Fig. 13(f), black and red lines) validates this phenomenon.

When the gear pair profile shift coefficients are identical (with consistent centre distance), comparing the combination where $X_{mc1} < 0$ and $X_{mc2} > 0$ to the combination where $X_{mc2} < 0$ and $X_{mc1} > 0$, the former results in improved K_a, K_b, and K_m, while K_{ppu} decreases. For example, comparing the combination $X_{mc1} = -0.4$, $X_{mc2} = 0.5$ with $X_{mc2} = -0.4$, $X_{mc1} = 0.5$ (as shown in Figs. 14(a), 14(b), and 14(c)), the former (blue solid lines - A1, A2, A3) exhibits higher K_a, K_b, and K_m values than the latter (blue dashed lines - B1, B2, B3). As shown in Fig. 14(d), the K_{ppu} of the former (blue solid line - A4) is lower than that of the latter (blue dashed line - B4).

A.2. $X_{mci} > 0$

As shown in Figs. 15(a), (c), and (e), the first three combinations are as follows: X_{mc1} values of 0.1, 0.2, and 0.3, with corresponding X_{mc2} ranges of 0.5-0.8, 0.4-0.7, and 0.3-0.6, respectively. In contrast, the last three combinations, shown in Figs. 15(b), (d), and (f), represent the reverse of these values.

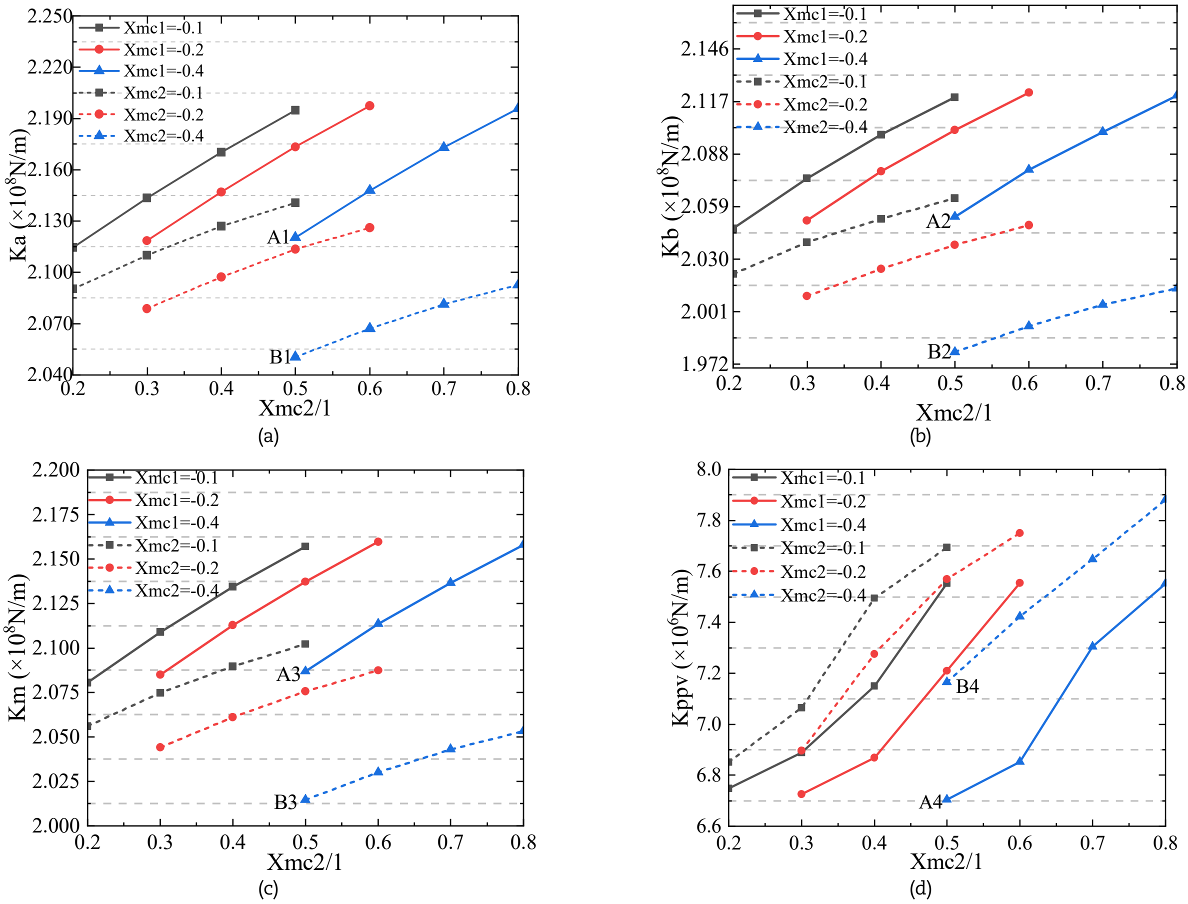

Fig. 14. Stiffness indicators, (a) Maximum stiffness, (b) Minimum stiffness, (c) Average stiffness, (d) Peak-to-peak stiffness.

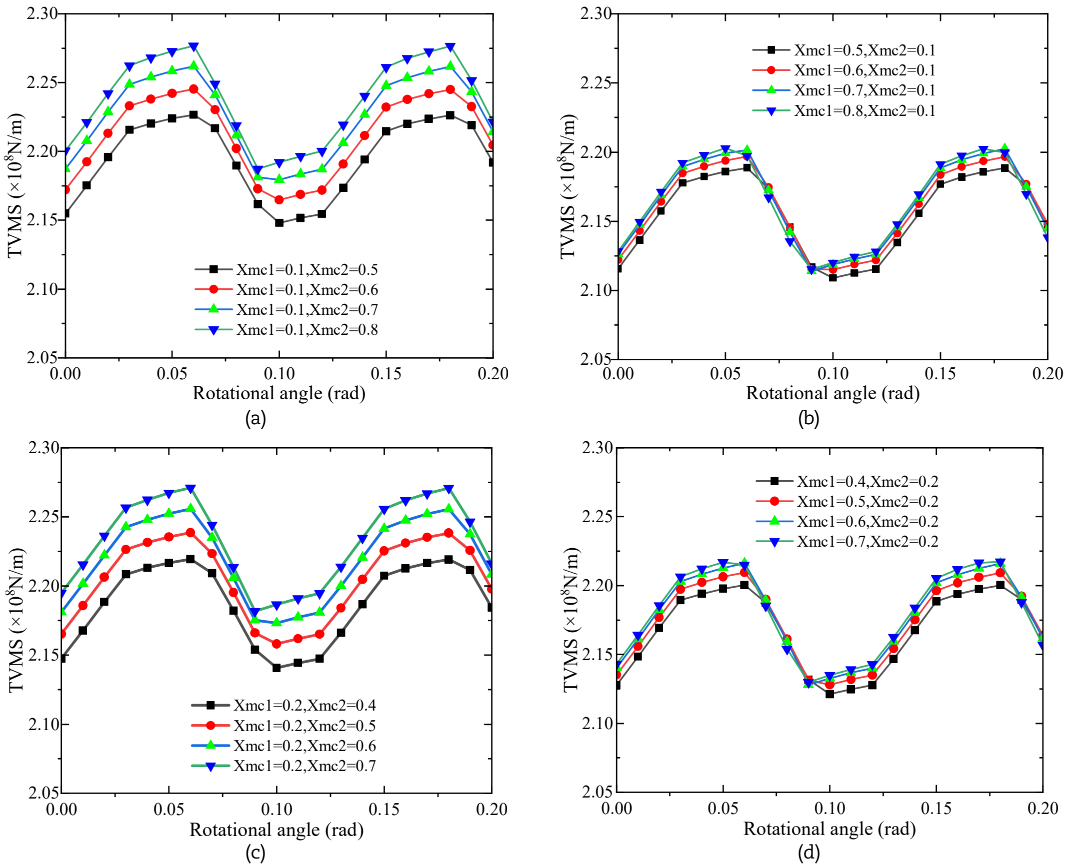

Fig. 15. TVMS with different modification coefficients.

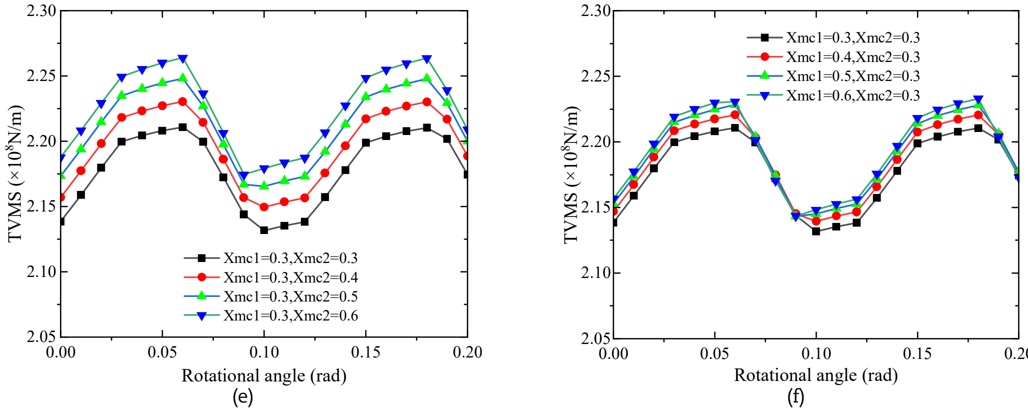

Fig. 15. Continued.

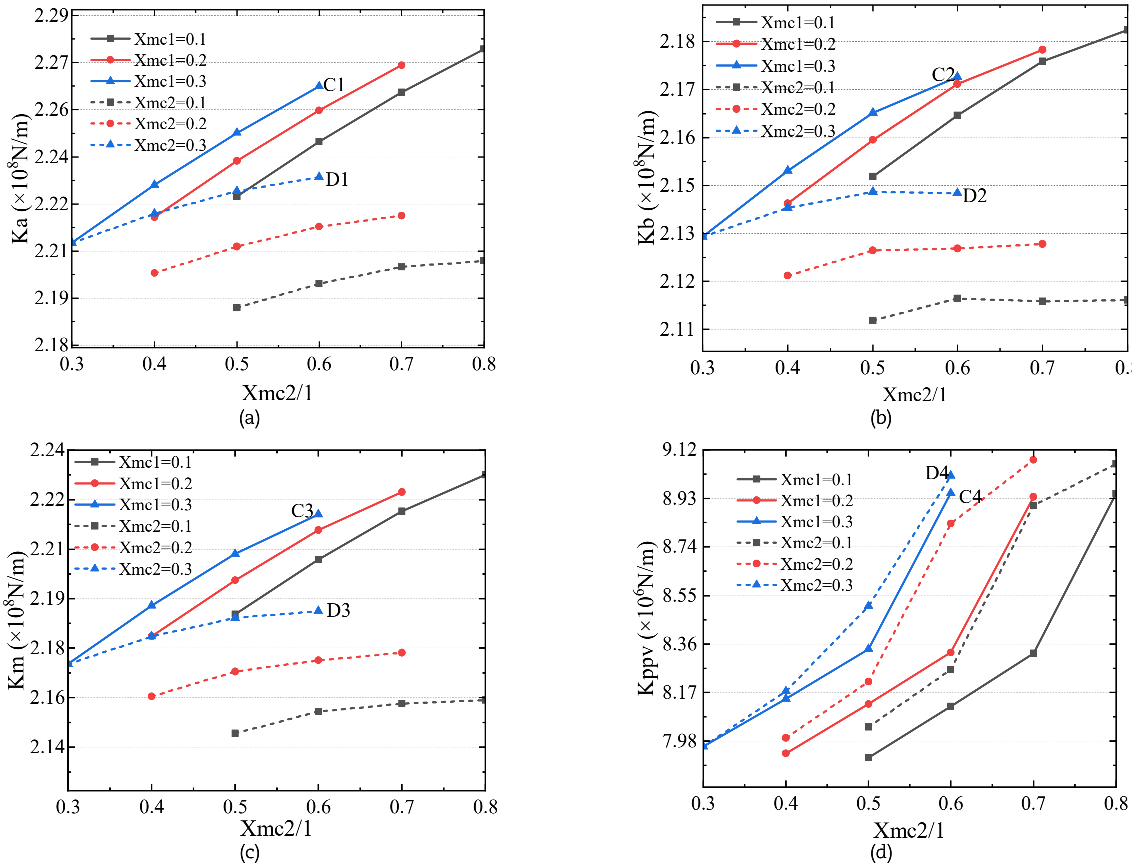

Fig. 16. Stiffness indicators, (a) Maximum stiffness, (b) Minimum stiffness, (c) Average stiffness, (d) Peak-to-peak stiffness.

As shown in Fig. 15, when the gear pair profile shift coefficients are identical (with consistent centre distance), the overall meshing stiffness is higher when $0 < X_{mc1} < X_{mc2}$ than when $0 < X_{mc2} < X_{mc1}$. For instance, the meshing stiffness of the combination $X_{mc1} = 0.3$, $X_{mc2} = 0.6$ (blue line in Fig. 15(e)) is higher than that of $X_{mc2} = 0.3$, $X_{mc1} = 0.6$ (blue line in Fig. 15(f)).

Under identical conditions of equal growth rate in the sum of the helical gear pair profile shift coefficients (i.e., an equal increase in centre distance), the overall meshing stiffness shows a greater improvement when $X_{mc1} > 0$ (constant) and $X_{mc2} > 0$ (gradually increasing) than when $0 < X_{mc2}$ (constant) and $0 < X_{mc1}$ (gradually increasing). For instance, the meshing stiffness improvement of the combination $X_{mc1} = 0.3$, $X_{mc2} = 0.5/0.6$ (green and blue lines in Fig. 15(e)) is greater than that of the combination $X_{mc2} = 0.3$, $X_{mc1} = 0.5/0.6$ (green and blue lines in Fig. 15(f)).

As shown in Fig. 16, under identical gear pair profile shift coefficients (with consistent centre distances), the overall K_a, K_b and K_m are higher when $0 < X_{mc1} < X_{mc2}$ than when $0 < X_{mc2} < X_{mc1}$; however, the K_{ppv} is lower in the former case. For instance, the combination $X_{mc1} = 0.3$, $X_{mc2} = 0.6$ (blue solid lines - C1, C2, C3) exhibits higher K_a, K_b, and K_m values than the combination $X_{mc2} = 0.3$, $X_{mc1} = 0.6$ (blue dashed lines - D1, D2, D3), as shown in Figs. 16(a), 16(b), and 16(c). Additionally, the K_{ppv} of the former (blue solid line - C4) is lower than that of the latter (blue dashed line - D4), as shown in Fig. 16(d).

4.2. Negative profile shift of helical gear

B.1. $X_{mci} > 0$ & $X_{mci} < 0$

As shown in Figs. 17(a), (c), and (e), the first three combinations are: X_{mc1} is 0.1, 0.2, and 0.4, respectively, while X_{mc2} corresponds to -0.2 to -0.5, -0.3 to -0.6, and -0.5 to -0.8, respectively. As shown in Figs. 17(b), (d), (f), the last three combinations are the reverse.

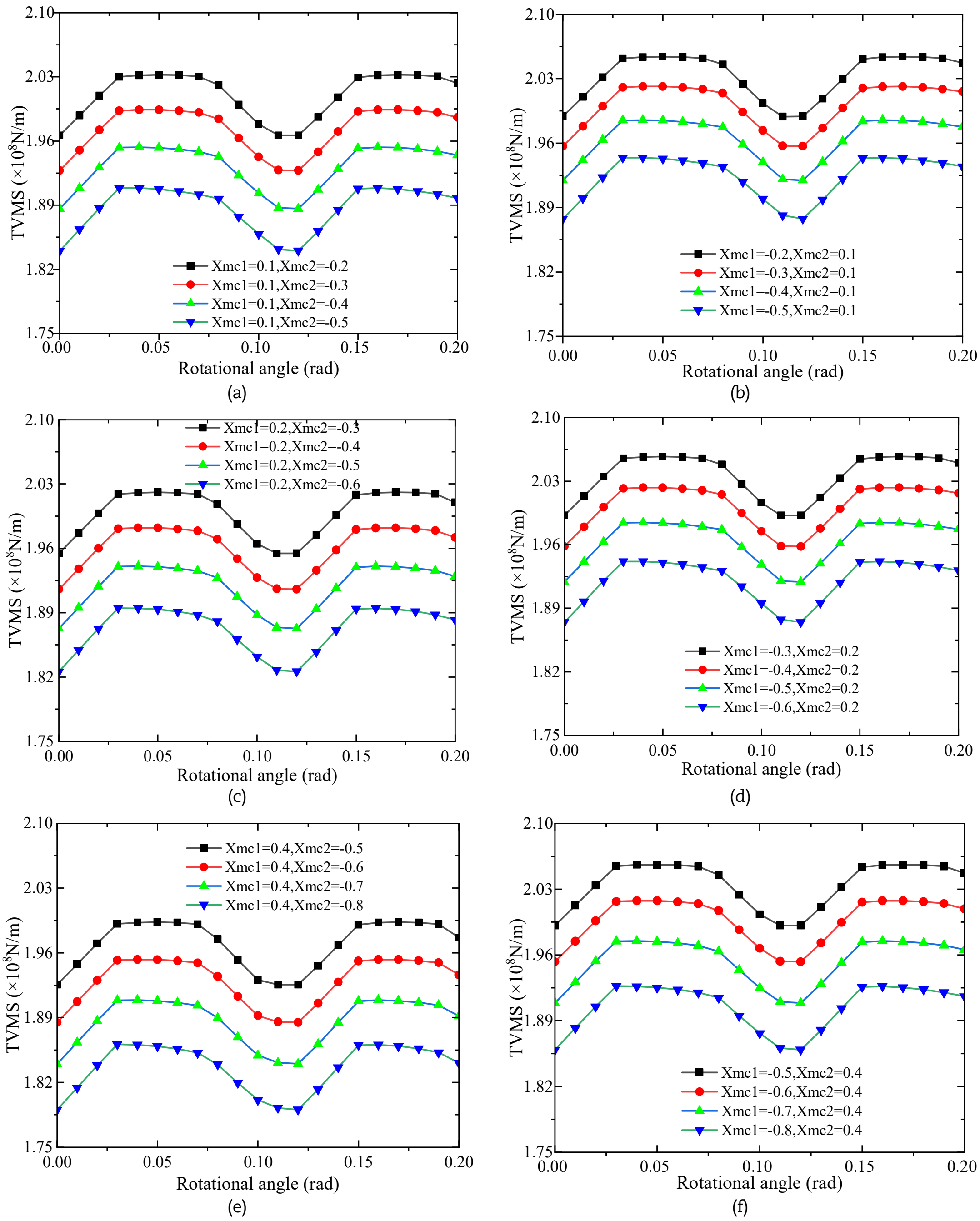

Fig. 17. TVMS with different modification coefficients.

As shown in Fig. 17, when the sum of the gear pair profile modification coefficients is identical (with consistent centre distance), the overall meshing stiffness is higher when $X_{mc1} < 0$ and $X_{mc2} > 0$ than when $X_{mc2} < 0$ and $X_{mc1} > 0$. For instance, the meshing stiffness of the combination $X_{mc1} = -0.5$, $X_{mc2} = 0.4$ (black line in Fig. 17(f)) is higher than that of the combination $X_{mc1} = 0.4$, $X_{mc2} = -0.5$ (black line in Fig. 17(e)).

Under conditions where the increase in the helical gear pair's profile modification coefficient (i.e., the increase in centre distance) is consistent, the increase in meshing stiffness is greater when $X_{mc1} > 0$ (constant) and $X_{mc2} < 0$ (gradually increasing) and when $X_{mc2} > 0$ (constant) and $X_{mc1} < 0$ (gradually increasing).

For instance, the increase in meshing stiffness of the combination $X_{mc1} = 0.4$, $X_{mc2} = -0.6/-0.5$ (red and black lines in Fig. 17(e)) is approximately equal to that of the combination $X_{mc2} = 0.4$, $X_{mc1} = -0.6/-0.5$ (red and black lines in Fig. 17(f)), showing similar trends.

As shown in Fig. 18, under identical gear pair profile modification coefficients (with consistent centre distances), the overall K_a, K_b, and K_m are higher when $X_{mc1} < 0$ and $X_{mc2} > 0$ than when $X_{mc2} < 0$ and $X_{mc1} > 0$; however, K_{ppv} is lower in the former case. For instance, the combination $X_{mc1} = -0.5$, $X_{mc2} = 0.4$ (blue dashed lines - E1, E2, E3) exhibits higher K_a, K_b, and K_m values than the combination $X_{mc2} = -0.5$, $X_{mc1} = 0.4$ (blue solid lines - F1, F2, F3), as shown in Figs. 18(a), (b), and (c). Additionally, the K_{ppv} of the former (blue dashed line - E4) is lower than that of the latter (blue solid line - F4), as shown in Fig. 18(d).

B.2. $X_{mci} < 0$

As shown in Figs. 19(a), (c), and (e), the first three combinations are as follows: X_{mc1} values are -0.1, -0.2, and -0.3, respectively, while X_{mc2} ranges from -0.3 to -0.6, -0.2 to -0.5, and -0.1 to -0.4, respectively. Figures 19(b), (d), and (f) display the last three combinations, which are the reverse of the first.

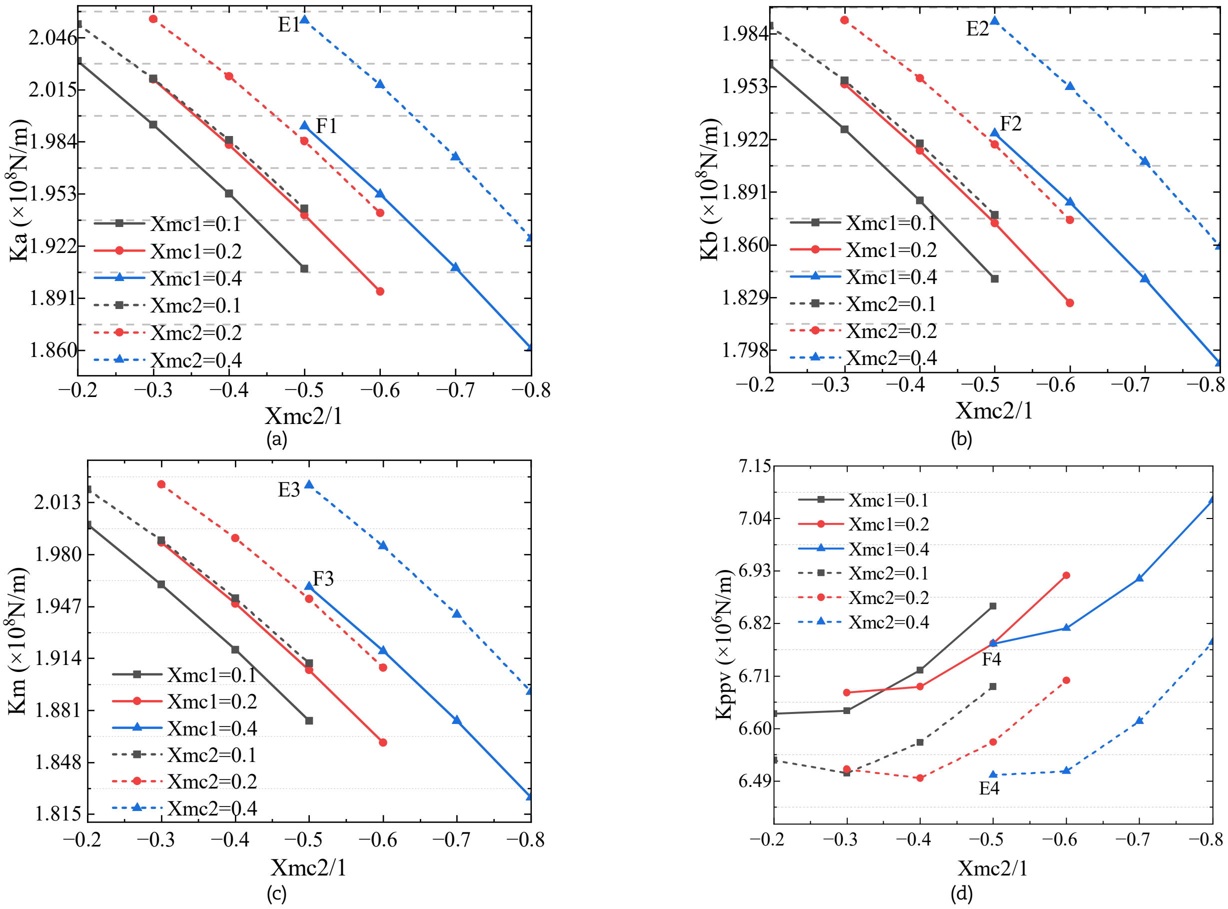

Fig. 18. Stiffness indicators, (a) Maximum stiffness, (b) Minimum stiffness, (c) Average stiffness, (d) Peak-to-peak stiffness.

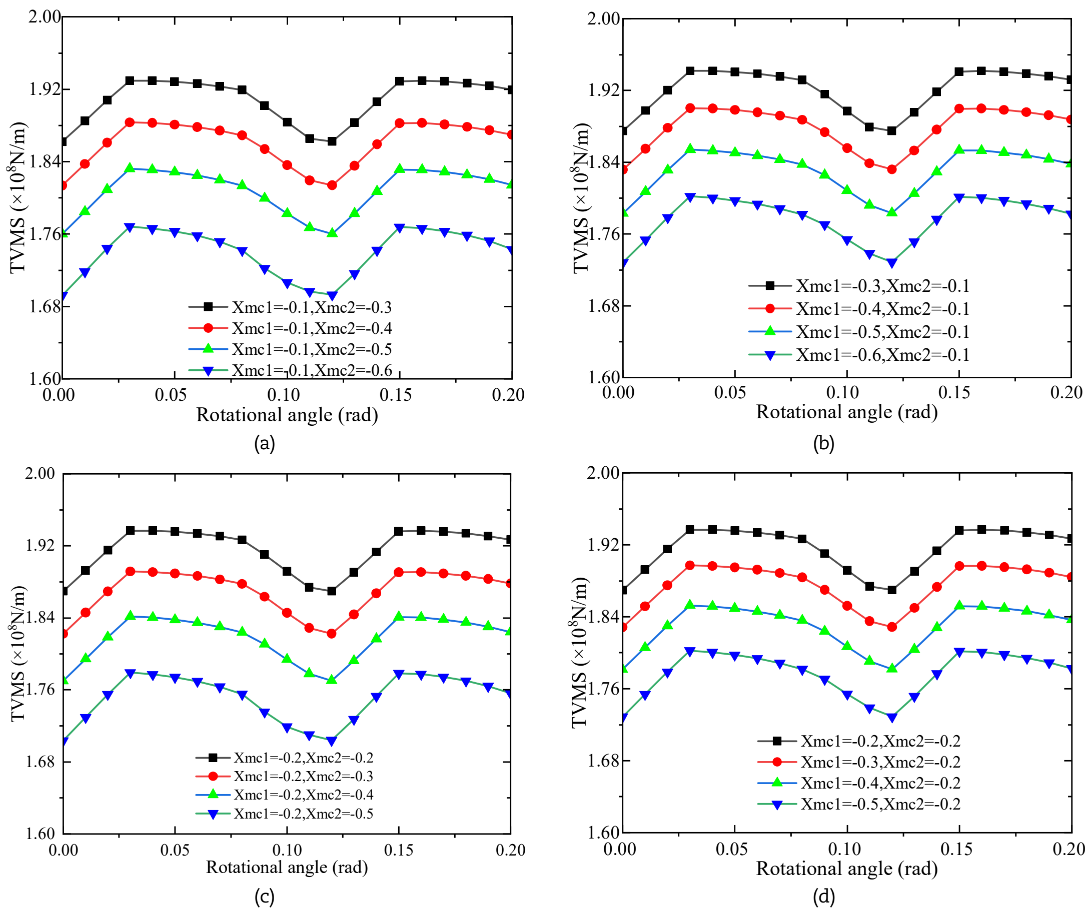

Fig. 19. TVMS with different modification coefficients.

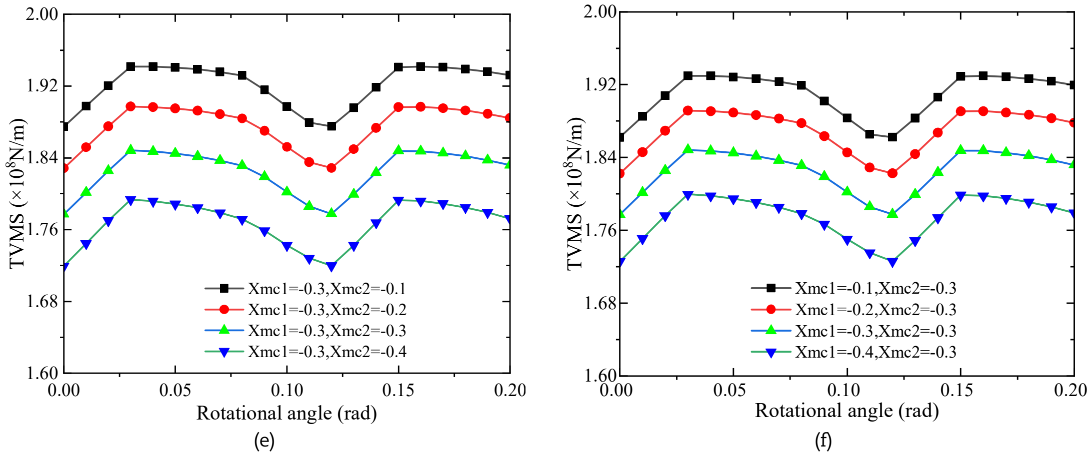

Fig. 19. Continued.

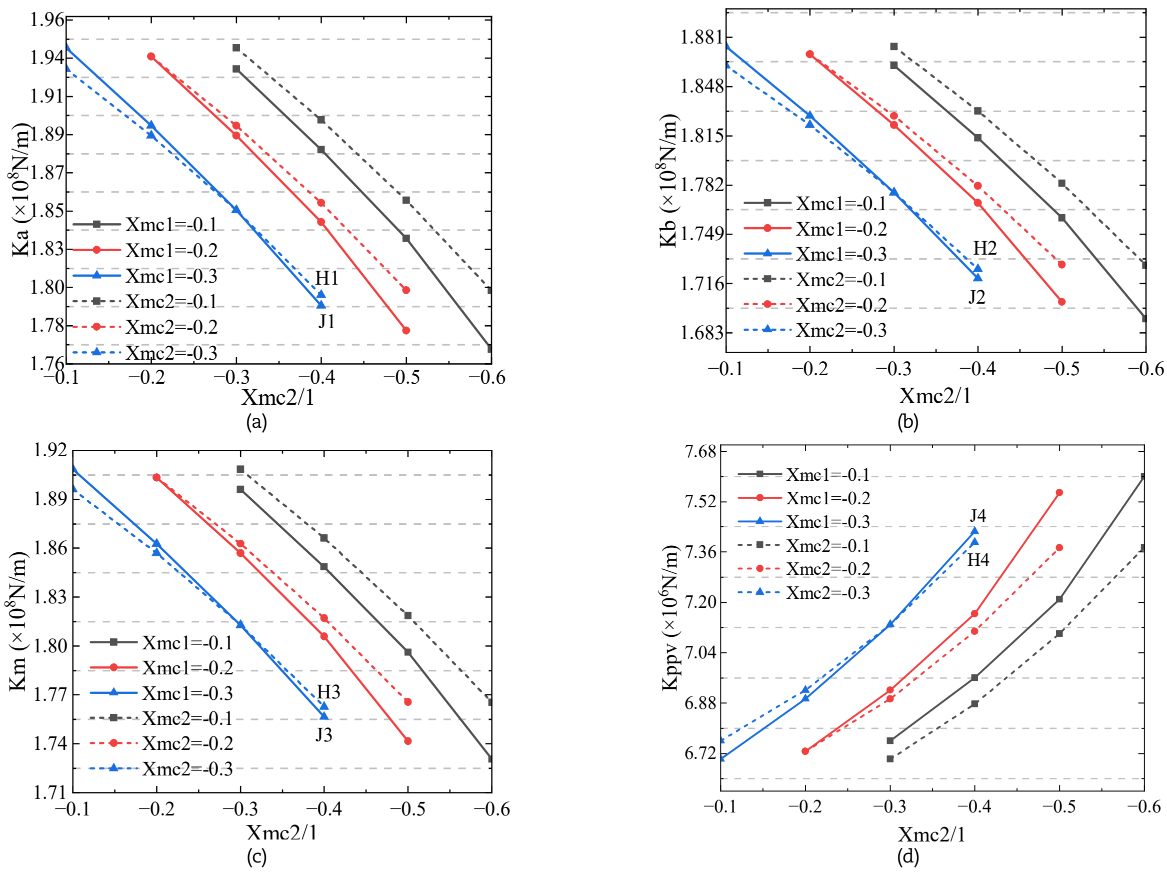

Fig. 20. Stiffness indicators, (a) Maximum stiffness, (b) Minimum stiffness, (c) Average stiffness, (d) Peak-to-peak stiffness.

As shown in Fig. 19, when the gear pair profile modification coefficients are identical (with a consistent centre distance), the overall meshing stiffness is higher when $X_{mc1} < X_{mc2} < 0$ than when $X_{mc2} < X_{mc1} < 0$. For instance, the meshing stiffness of the combination $X_{mc1} = -0.3$, $X_{mc2} = -0.1$ (black line in Fig. 19(e)) is higher than that of the combination $X_{mc2} = -0.3$, $X_{mc1} = -0.1$ (black line in Fig. 19(f)). Under identical conditions of equal increase in the profile shift coefficient of helical gear pairs (i.e., consistent centre distance), the overall meshing stiffness shows a more significant increase when $X_{mc1} < 0$ (constant) and $X_{mc2} < 0$ (gradually increasing) than when $X_{mc2} < 0$ (constant) and $X_{mc1} < 0$ (gradually increasing). For instance, the increase in meshing stiffness of the combination $X_{mc1} = -0.3$, $X_{mc2} = -0.2/-0.1$ (red and black lines in Fig. 19(e)) is more significant than that of the combination $X_{mc2} = -0.3$, $X_{mc1} = -0.2/-0.1$ (red and black lines in Fig. 19(f)).

As shown in Fig. 20, under identical gear pair profile shift coefficients (with a consistent centre distance), the overall K_a, K_b, and K_m are higher when $X_{mc1} < X_{mc2} < 0$ than when $X_{mc2} < X_{mc1} < 0$; however, the K_{ppv} is lower in the former case. For instance, the combination$X_{mc1} = -0.4$, $X_{mc2} = -0.3$ (blue dashed lines - H1, H2, H3) exhibits higher K_a, K_b, and K_m values than the combination $X_{mc1} = -0.3$, $X_{mc2} = -0.4$ (blue solid lines - J1, J2, J3), as shown in Figs. 20(a), (b), and (c). Additionally, the K_{ppv} of the former (blue dashed line - H4) is lower than that of the latter (blue solid line - J4), as shown in Fig. 20(d).

4.3. Zero profile shift of helical gear

As shown in Fig. 21(a), the former combination is: X_{mc1} (< 0) + X_{mc2} (> 0) = 0, and their sum equals 0. As shown in Fig. 21(b), the latter combination is: X_{mc1} (> 0) + X_{mc2} (< 0) = 0.

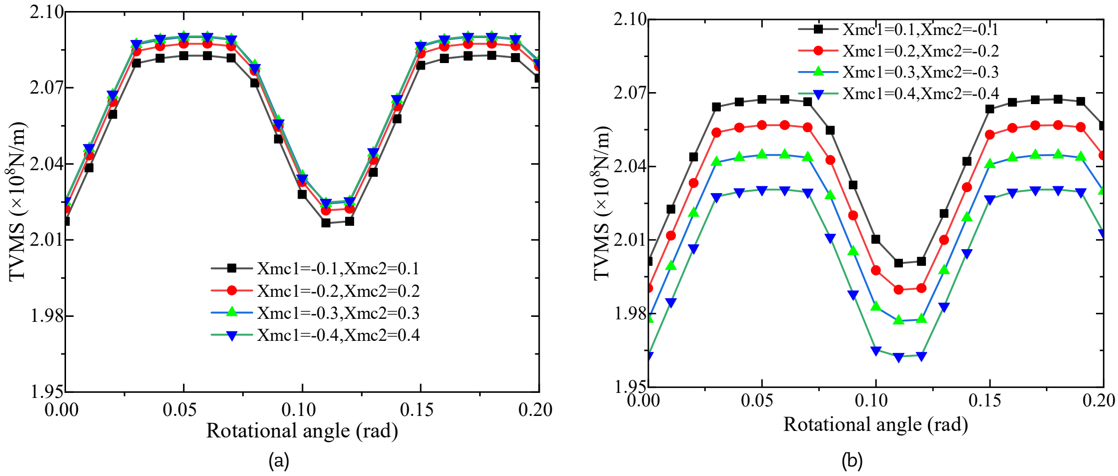

Fig. 21. TVMS with different modification coefficients.

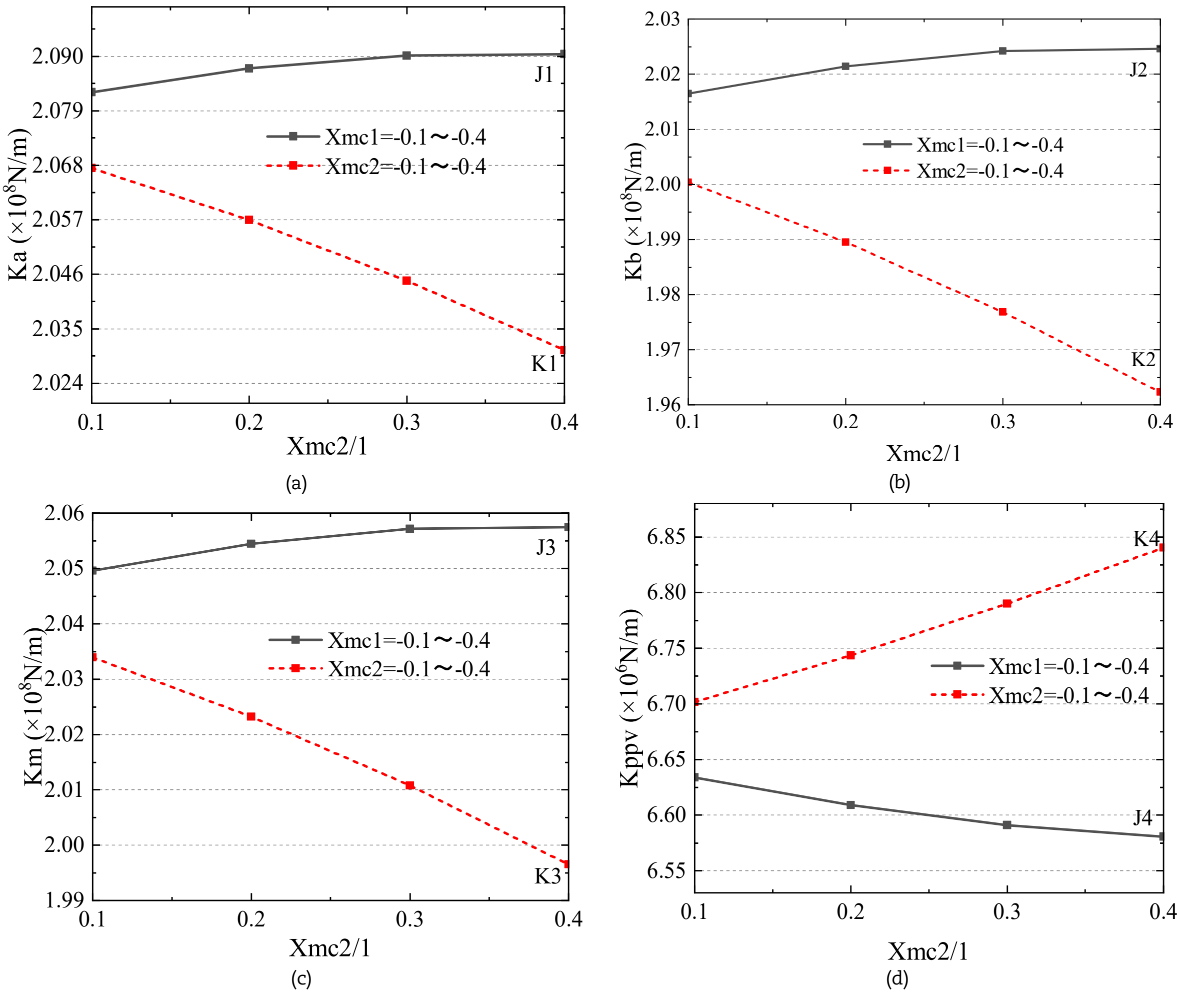

Fig. 22. Stiffness variation diagram, (a) Maximum stiffness, (b) Minimum stiffness, (c) Average stiffness, (d) Differential stiffness.

As shown in Fig. 21, when the helical gear pair profile modification coefficients are identical (with a consistent centre distance), the overall time-varying meshing stiffness is higher when $X_{mc1} < 0$ and $X_{mc2} > 0$ than when $X_{mc1} > 0$ and $X_{mc2} < 0$. For instance, the time-varying meshing stiffness of the combination $X_{mc1} = -0.4$, $X_{mc2} = 0.4$ (blue line in Fig. 21(a)) is higher than that of the combination $X_{mc1} = 0.4$, $X_{mc2} = -0.4$ (blue line in Fig. 21(b)).

As shown in Fig. 22, under identical helical gear pair profile shift coefficients (with a consistent centre distance), the overall K_a, K_b, and K_m are higher when$X_{mc1} < 0$ and $X_{mc2} > 0$ than when $X_{mc1} > 0$ and $X_{mc2} < 0$; however, the K_{ppv} is lower in the former case. For instance, the combination $X_{mc1} = -0.4$, $X_{mc2} = 0.4$ (black solid lines - J1, J2, J3) exhibits higher K_a, K_b, and K_m values than the combination $X_{mc1} = 0.4$, $X_{mc2} = -0.4$ (red dashed lines - K1, K2, K3), as shown in Figs. 22(a)-(c). Additionally, the K_{ppv} of the former (black solid line - J4) is lower than that of the latter (red dashed line - K4), as shown in Fig. 22(d).

5. Conclusion

This paper presented a TVMS analysis model for helical gears that incorporates profile shift, based on the potential energy method. The proposed model was designed to explore the impact of profile shift on gear meshing stiffness. The main conclusions are summarised as follows:

For both positive and negative profile shifting of helical gear pairs, among multiple groups of helical gear pairs with the same centre distance, when the profile modification coefficient of the pinion is smaller than that of the gear, the gear tooth body cross-sectional area increases, leading to a higher TVMS. Meanwhile, the maximum stiffness K_a, the minimum stiffness K_b, and average stiffness K_m are all improved, while the peak-to-peak stiffness K_{ppv} decreases; Among multiple groups of helical gear pairs with a consistent centre distance growth rate, the TVMS of the gear pair where the profile modification coefficient of the pinion remains constant and that of the gear gradually increases is higher. Additionally, the K_a, K_b, and K_m of this gear pair are larger, while the K_{ppv} is smaller.

For zero profile shifting of helical gear pairs: Among multiple groups of helical gear pairs with the same centre distance, when the profile shift coefficient of the pinion is smaller than that of the gear, the gear tooth body cross-sectional area of the gear pair increases, resulting in a higher TVMS. Moreover, the K_a, K_b, and K_m of this gear pair are larger, while the K_{ppv} is smaller.

In the future, relevant experiments will be conducted to further verify the above conclusions, and research on engineering applications will also be carried out.

Author contributions

All authors contributed to the study conception and design. Preparation, data collection and analysis were performed by Y. He and W. Zhang; The first draft of the manuscript was written by L. Bu; Research review were performed by L. Bu and B. Tan; J. Liu and D. Zhang supervised the findings of this work. The manuscript was written through the contribution of all authors. All authors discussed the results, reviewed, and approved the final version of the manuscript.

Acknowledgement

Not applicable.

Conflict of Interest

The authors declared no potential conflicts of interest concerning the research, authorship, and publication of this article.

Funding

The research was funded by Major Scientific and Technological Research Project in Hunan Province: 2025QK2005, Hunan Province Key Research and Development Plan-City-Provincial Collaboration Project: 2024QY2009, Major Science and Technology Projects of Hunan Province: 2023GK1030, 2025 Hunan Advanced Manufacturing 'Challenge-Driven Leadership' Project: 2025GXZH003.

Data Availability Statements

The datasets generated and/or analyzed during the current study are available from the corresponding author on reasonable request.

Appendix A

Stiffness calculations employ angular profile shift, based on the characteristics of the transition curve and involute curve that account for profile shift. $x_{\psi 1}$, $y_{\psi 1}$, x_1, y_1, x_2, y_2, I_{y1}, I_{y2}, A_{y1}, A_{y2}, $dy_1/d\gamma$, $dy_2/d\varepsilon$, denote functions of angular profile shift γ, ψ_1, or ε, respectively, expressed as:

$$x_{\psi_1} = r_b\left[(\psi_1+\theta_c)\cos\psi_1 - \sin\psi_1\right] \tag{A.1}$$

$$y_{\psi_1} = r_b\left[(\psi_1+\theta_c)\cos\psi_1 + \sin\psi_1\right] \tag{A.2}$$

$$x_1 = r\times\sin(\Phi) - \left(a_1/\sin\gamma + r_\rho\right)\times\cos(\gamma-\Phi) \tag{A.3}$$

$$y_1 = r\times\cos(\Phi) - \left(a_1/\sin\gamma + r_\rho\right)\times\sin(\gamma-\Phi) \tag{A.4}$$

$$x_2 = r_b\left[(\varepsilon+\theta_c)\cos\varepsilon - \sin\varepsilon\right] \tag{A.5}$$

$$y_2 = r_b\left[(\varepsilon+\theta_c)\cos\varepsilon + \sin\varepsilon\right] \tag{A.6}$$

$$A_{y1} = 2x_1L,\ A_{y2} = 2x_2L \tag{A.7}$$

$$I_{y1} = \frac{2}{3}x_1^3L,\ I_{y2} = \frac{2}{3}x_2^3L \tag{A.8}$$

$$\frac{\mathrm{d}y_1}{\mathrm{d}\gamma}=\frac{a_1\sin\left(\dfrac{a_1/\tan\gamma+b_1}{r}\right)\left(1+\tan^2\gamma\right)}{\tan^2\gamma}+\frac{a_1\cos\gamma}{\sin^2\gamma}\sin\left(\gamma-\frac{a_1/\tan\gamma+b_1}{r}\right)-\left(\frac{a_1}{\sin\gamma}+r_\rho\right)\cos\left(\gamma-\frac{a_1/\tan\gamma+b_1}{r}\right)\left(1+\frac{a_1\left(1+\tan^2\gamma\right)}{r\tan^2\gamma}\right) \tag{A.9}$$

$$\frac{\mathrm{d}y_2}{\mathrm{d}\varepsilon}=r_\mathrm{b}\left(\varepsilon+\theta_\mathrm{b}\right)\cos\varepsilon \tag{A.10}$$

where, θ_b is the half tooth angle on the gear base circle as:

$$\theta_\mathrm{b}=\left(\frac{\pi}{2}+2x_{mc}\tan\alpha\right)/Z+\mathrm{inv}\,\alpha. \qquad G=\frac{E}{2(1+\nu)} \tag{A.11}$$

Appendix B: Notation

m	Module
β	Helix angle
Z	Number of teeth
r	Pitch circle radius of the gear
r_a	Top circle radius
r_b	Base circle radius
r_c	Radius of the initial circle of the involute curve
r_p	Radius of the initial circle of the involute curve
α	Pressure angle of the pitch circle
x_{mc}	Gear profile shift coefficient
x_{mc1}	The modification coefficient of the pinion
x_{mc2}	The modification coefficient of the gear
h_a	Tip coefficient
c	Tip clearance coefficient
α_i	Pressure angle at any point on the involute curve
α_c	Pressure angle of the involute curve
α_a	Pressure angle of the involute tip circle
L	Width of the sliced tooth
I_{y1}, I_{y2}	Area moment of inertia
A_{y1}, A_{y2}	Cross-sectional areas at distances y1 and y2 from the origin
x_1, x_2	Vertical coordinates of any point on the transition curve and involute curve
x_β	Distance between the contact point and the gear centerline
y_β	Horizontal distance between the contact point and the origin
y_1, y_2	Horizontal coordinates of any point on the transition curve and the involute curve
y_C, y_D	Starting and ending points of the transition curve CD
k_a, k_b, k_h, k_s, k_f	Stiffness values for compression, bending, Hertzian contact, shear, and base material
ε_i	Angular profile shift at any point on the curve
ε_c	Angular profile shift at point C
γ_β	Axial contact ratio
γ_α	Tangential contact ratio
γ_ε	Total contact ratio
E	Young's modulus
G	Shear modulus
υ	Poisson's ratio
K_a	Maximum stiffness
K_b	Minimum stiffness
K_m	Average stiffness
K_{ppv}	Peak-to-peak stiffness

References

[1] Öztürk, V.Y., Cigeroglu, E., Özgüven, H.N., Ideal tooth profile modifications for improving nonlinear dynamic response of planetary gear trains, *Journal of Sound and Vibration*, 500, 2021, 116007.

[2] Tan, B., Deng, Z., Liu, J., Li, C., Tan, Y., Ning, D., He, Y., Energy-Conserving Nonlinear Active Control for a Bird-Inspired Quasi-Zero Stiffness Stretcher Vibration Isolation System with Asymmetric Stiffness, *International Journal of Structural Stability and Dynamics*, 2025.

[3] Jun, Z., Wei-min, T., Qin, C., Tao, C., Reliability Sensitivity Analysis of Tooth Modification on Dynamic Transmission Error of Helical Planetary Gears, *Proceedings of the Institution of Mechanical Engineers, Part C: Journal of Mechanical Engineering Science*, 234(19), 2020, 3903–3918.

[4] Lian, Z., Xiao, Z., Li, C., Zhou, T., Study on the Dynamic Characteristics of Planetary Gear System Considering Motor Torque Ripple and Suppression Strategy, *International Journal of Applied Mechanics*, 17(5), 2025, 2550040.

[5] Liu, Y., Shi, Z., Shen, G., Zhen, D., Wang, F., Evaluation Model of Mesh Stiffness for Spur Gear with Tooth Tip Chip Fault, *Mechanism and Machine Theory*, 158, 2021, 104238.

[6] Huang, W., Hu, H., Ma, H., Dynamic Modeling and Response Analysis of Cracked Herringbone Gear Transmission Systems with Installation Errors, *Mechanism and Machine Theory*, 206, 2025, 105924.

[7] Raghuwanshi, N.K., Parey, A., Experimental Measurement of Mesh Stiffness by Laser Displacement Sensor Technique, *Measurement*, 128, 2018, 63–70.

[8] Chen, K., Ma, H., Che, L., Comparison of Meshing Characteristics of Helical Gears with Spalling Fault Using Analytical and Finite-Element Methods, *Mechanical Systems and Signal Processing*, 121, 2019, 279–298.

[9] Liang, X., Zhang, H., Zuo, M.J., Three New Models for Evaluation of Standard Involute Spur Gear Mesh Stiffness, *Mechanical Systems and Signal Processing*, 101, 2018, 424–434.

[10] Dai, H., Long, X., Chen, F., An Improved Analytical Model for Gear Mesh Stiffness Calculation, *Mechanism and Machine Theory*, 159, 2021, 104262.

[11] Li, H., Tang, J., Chen, S., Ding, H., Sun, Z., Rong, K., Analytical calculation of mesh stiffness for spiral bevel gears with an improved global tooth deformation model, *Mechanism and Machine Theory*, 191, 2024, 105492.

[12] Zou, H., Wang, S., He, Q., Analytical Algorithm for Time-Varying Meshing Stiffness of Modified Herringbone Gears, *Journal of Northwestern Polytechnical University*, 40(3), 2022, 538–548.
[13] Wang, Q., Zhao, B., Fu, Y., An Improved Time-Varying Mesh Stiffness Model for Helical Gear Pairs Considering Axial Mesh Force Component, *Mechanical Systems and Signal Processing*, 106, 2018, 413–429.
[14] Wan, Z., Cao, H., Zi, Y., Mesh Stiffness Calculation Using an Accumulated Integral Potential Energy Method and Dynamic Analysis of Helical Gears, *Mechanism and Machine Theory*, 92, 2015, 447–463.
[15] Feng, M., Ma, H., Li, Z., An Improved Analytical Method for Calculating Time-Varying Mesh Stiffness of Helical Gears, *Meccanica*, 53(4), 2018, 1131–1145.
[16] Yang, H., Shi, W., Chen, Z., An Improved Analytical Method for Mesh Stiffness Calculation of Helical Gear Pair Considering Time-Varying Backlash, *Mechanical Systems and Signal Processing*, 170, 2022, 108882.
[17] Shi, J.F., Han, C., Chen, L.X., Investigating wear-induced health-instability dynamics in spur gear systems with installation error, *Nonlinear Dynamics*, 2025, 1–22.
[18] Chung, W.J., Park, J.H., Yoo, H.G., Improved Analytical Model for Calculating Mesh Stiffness and Transmission Error of Helical Gears Considering Trochoidal Root Profile, *Mechanism and Machine Theory*, 163, 2021, 104386.
[19] Shi, J.F., Gou, X.F., Zhu, L.Y., Five-state engaging model and dynamics of gear-rotor-bearing system based on time-varying contact analysis considering gear temperature and lubrication, *Applied Mathematical Modelling*, 112, 2022, 47–77.
[20] Xiong, Y., Huang, K., Xu, F., Research on the Influence of Backlash on Mesh Stiffness and the Nonlinear Dynamics of Spur Gears, *Applied Sciences*, 9(5), 2019, 1029.
[21] Ma, H., Feng, M., Li, Z., Time-Varying Mesh Characteristics of a Spur Gear Pair Considering the Tip-Fillet and Friction, *Meccanica*, 52(7), 2017, 1695–1709.
[22] Chen, Z., Zhou, Z., Zhai, W., Improved Analytical Calculation Model of Spur Gear Mesh Excitations with Tooth Profile Deviations, *Mechanism and Machine Theory*, 149, 2020, 103838.
[23] Ma, H., Pang, X., Feng, R., Evaluation of Optimum Profile Modification Curves of Profile Shifted Spur Gears Based on Vibration Responses, *Mechanical Systems and Signal Processing*, 70, 2016, 1131–1149.
[24] Wang, J., Yang, J., Lin, Y., He, Y., Analytical Investigation of Profile Shifts on the Mesh Stiffness and Dynamic Characteristics of Spur Gears, *Mechanism and Machine Theory*, 167, 2022, 104529.
[25] Tan, L., Hu, Z., Tang, J., Sun, Z., Wang, Z., Dynamic Characteristics Analysis of Profile-Shifted Planetary Gears Considering Friction, *Meccanica*, 59(2), 2024, 193–215.
[26] Yu, W., Mechefske, C.K., Timusk, M., Influence of the Addendum Modification on Spur Gear Back-Side Mesh Stiffness and Dynamics, *Journal of Sound and Vibration*, 389, 2017, 183–201.
[27] Sainsot, P., Velex, P., Duverger, O., Contribution of Gear Body to Tooth Deflections - A New Bidimensional Analytical Formula, *Journal of Mechanical Design*, 126(4), 2004, 748–752.
[28] Zheng, J., Qin, D., Liu, C., A Novel Dynamic Modeling Method with Slice Coupling for Thin-Rimmed Gear Transmission, *Acta Mechanica*, 234(12), 2023, 6097–6121.

ORCID iD

Lei Bu https://orcid.org/0009-0007-4489-9061

How to cite this article: Bu L. et al., Study on the Effect of Profile Shifts on the Meshing Stiffness of Helical Gears, *J. Appl. Comput. Mech.*, xx(x), 2026, 1–19. https://doi.org/10.22055/jacm.2026.48790.5501